Theor Chem Acc (2005) 113: 287–293
DOI 10.1007/s00214-005-0671-y

REGULAR ARTICLE

M. Kohout · K. Pernal · F. R. Wagner · Yu. Grin

Electron localizability indicator for correlated wavefunctions. II Antiparallel-spin pairs

Received: 14 October 2004 / Accepted: 24 March 2005 / Published online: 6 May 2005

Abstract The electron localizability indicator for anti parallel-spin pairs is closely associated with the correlation of the motion of opposite-spin electrons. At the Hartree–Fock level this functional is constant throughout the whole space, whereas for correlated wavefunctions structures resembling atomic shells and the bonding situation emerges.

Keywords Electron localizability indicator · Configuration interaction · Correlation

1 Introduction

In the preceeding paper [1], denoted in the following as Part I, the electron localizability indicator for same-spin electron pairs (ELI) at the correlated level was introduced and its relation to the electron localization functions (ELF) of Becke and Edgecombe [2] and of Savin et al. [3], respectively, was illustrated.

Electron pairs provides signatures of chemical bonding in direct space. In the ELI picture a bond is connected with spatial region where the motion of same-spin electrons is highly correlated, which leads to a local decrease of the same-spin electron pairing. Conceptually, this cannot be easily translated into the Lewis picture of chemical bonding [4], where the bonding electrons are expected to form pairs. The reason is that an unequivocal mutual interrelation between the extent of pairing for the respective same-spin and opposite-spin electrons is not evident. This is especially obvious at the Hartree–Fock (HF) level, where the opposite-spin electrons are "uncorrelated" (in the sense, that the number of opposite-spin electron pairs equals the product of the charges for the respective spins), thus yielding the same extent of opposite-spin electron pairing all over the space.

Following the recently given derivation of the ELI [5] it is straightforward to extend this approach to the electron localizability indicator for antiparallel-spin pairs (ELIA) utilizing the opposite-spin electron pair density. ELIA describes the local pairing of opposite-spin electrons and therefore provides the natural solution to this conceptual dilemma. In this context it may be interpreted as the quantum mechanical counterpart of the simple Lewis model of chemical bonding.

M. Kohout (✉) · F. R. Wagner · Y. Grin
Max-Planck-Institut für Chemische Physik fester Stoffe, Nöthnitzer Str. 40, 01187 Dresden, Germany
E-mail: kohout@cpfs.mpg.de

K. Pernal
Institute of Physics, University of Szczecin, Wielkopolska 15, 70-451 Szczecin, Poland

2 Theory

As in Part I, we consider an N-electron wavefunction that determines the spinless one- and two-electron reduced density matrices $\rho_1(\vec{r}_1' \mid \vec{r}_1)$ and $\rho_2(\vec{r}_1'\vec{r}_2' \mid \vec{r}_1\vec{r}_2)$, respectively, the diagonal part of which are the electron density $\rho(\vec{r}_1)$ and the electron pair density $\rho_2(\vec{r}_1, \vec{r}_2)$ [6–8]. We decompose the electron density, which is normalized to the total number of electrons N, into the spin components ρ_α and ρ_β:

$$\rho(\vec{r}) = \rho_\alpha(\vec{r}) + \rho_\beta(\vec{r}). \tag{1}$$

The pair density, which is normalized to the number of electron pairs (N-1)N/2, can be written using four spin components:

$$\rho_2(\vec{r}_1, \vec{r}_2) = \rho_2^{\alpha\alpha}(\vec{r}_1, \vec{r}_2) + \rho_2^{\beta\beta}(\vec{r}_1, \vec{r}_2) + \rho_2^{\alpha\beta}(\vec{r}_1, \vec{r}_2) + \rho_2^{\beta\alpha}(\vec{r}_1, \vec{r}_2)\,. \tag{2}$$

Analogously to the derivation of ELI [5], the whole space is divided into compact space filling mutually exclusive regions. In Fig. 1 three such regions are displayed (there are of course other adjacent regions that are not shown in the diagram). The regions $\Omega_{q,a}$, $\Omega_{q,b}$, and $\Omega_{q,c}$ are referenced by arbitrary points $\vec{r}_a$, $\vec{r}_b$, and $\vec{r}_c$ inside the respective regions. In each region the charge product $q_\alpha q_\beta$ (with the respective charges q_α and q_β for the α-spin and β-spin electrons contained in the region) is fixed at a small arbitrary (but constant for all regions) value. This fixed charge condition, that controls the volume of the regions, is indicated by the subscript

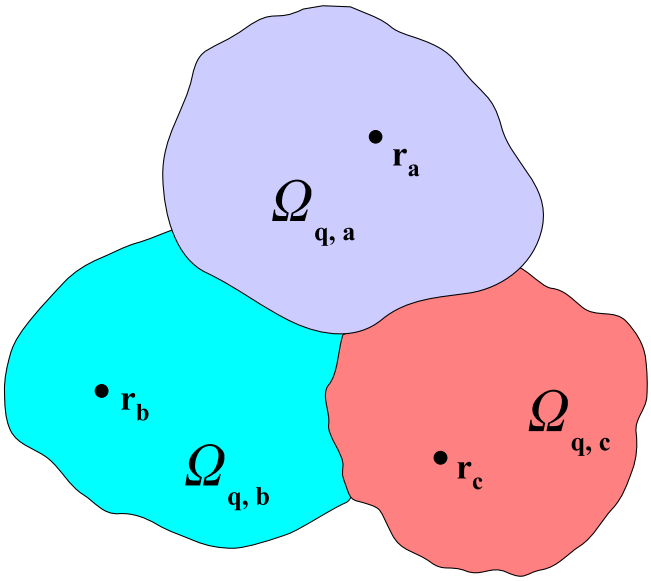

Fig. 1 Three adjacent regions $\Omega_{q,a}$, $\Omega_{q,b}$, and $\Omega_{q,c}$ (referenced by the respective points $\vec{r}_a$, $\vec{r}_b$, and $\vec{r}_c$) controlled by the fixed charge product condition

q (because in our restricted populations approach different controlling conditions are conceivable).

In our approach (see below), the correlation of the motion of the opposite-spin electrons is reflected by the $q_{\alpha\beta}$-restricted pair population $\zeta_q^{\alpha\beta}(\vec{r}_a)$:

$$\zeta_q^{\alpha\beta}(\vec{r}_a) \;=\; \iint\limits_{\Omega_{q,a}} \rho_2^{\alpha\beta}(\vec{r}_1,\vec{r}_2)\; d\vec{r}_1 d\vec{r}_2\,, \tag{3}$$

that is, the opposite-spin pair population in the region $\Omega_{q,a}$ under the restriction that the charge contained in the $\Omega_{q,a}$ yields the fixed value $q_\alpha q_\beta$. Here, we use the idea that the electron pair population of "uncorrelated" opposite-spin pairs is given by the product of the α-spin and β-spin charges, $q_\alpha q_\beta$ (i.e., the electron pair probability is given by the product of the corresponding single electron probabilities [9]).

At the HF level of theory the opposite-spin electron pair density is simply given by the product of the respective α-spin and β-spin densities, that is, in the above sense the motion of the opposite-spin electrons is "uncorrelated":

$$\rho_2^{\alpha\beta}(\vec{r}_1,\vec{r}_2) = \frac{1}{2}\rho_\alpha(\vec{r}_1)\rho_\beta(\vec{r}_2). \tag{4}$$

It is clear, that in this "uncorrelated" case, the $q_{\alpha\beta}$-restricted pair population, that is, the integral of $\rho_2^{\alpha\beta}(\vec{r}_1,\vec{r}_2)$ over $\Omega_{q,a}$ yields a constant value for all the regions. This is also true for any one-determinantal ansatz, for example, using Kohn-Sham orbitals from a density functional calculation.

For correlated wavefunctions the opposite-spin electron pair density reads:

$$\rho_2^{\alpha\beta}(\vec{r}_1,\vec{r}_2) = \frac{1}{2}\rho_\alpha(\vec{r}_1)\rho_\beta(\vec{r}_2)\left[1 + f^{\alpha\beta}(\vec{r}_1,\vec{r}_2)\right], \tag{5}$$

with the correlation factor $f^{\alpha\beta}(\vec{r}_1,\vec{r}_2)$. Now, the $q_{\alpha\beta}$-restricted pair population can attain values different from the product $q_\alpha q_\beta$. The motion of the opposite-spin electrons becomes correlated in the above sense.

Using the same configuration interaction (CI) ansatz for the wavefunction as in Part I yields for the opposite-spin component $\rho_2^{\alpha\beta}(\vec{r}_1,\vec{r}_2)$ of the electron pair density:

$$\rho_2^{\alpha\beta}(\vec{r}_1,\vec{r}_2) = \frac{1}{2}\sum_{i,k}^{\alpha}\sum_{j,l}^{\beta} P_{ij,kl}\;\left|\phi_i(\vec{r}_1)\phi_j(\vec{r}_2)\right|\;\left|\phi_k(\vec{r}_1)\phi_l(\vec{r}_2)\right|, \tag{6}$$

with the coefficients $P_{ij,kl}$ of the two-electron reduced density matrix.

To search for the regions controlled by the fixed charge condition as well as the evaluation of the corresponding pair populations over those regions would be a tremendous task. To circumvent this handicap we exploit the possibility to approximate the $q_{\alpha\beta}$-restricted pair population $\zeta_{q,CI}^{\alpha\beta}(\vec{r}_a)$ by the integral of the Taylor expansion of $\rho_2^{\alpha\beta}(\vec{r}_1,\vec{r}_2)$ around the position $\vec{r}_a$ over the region $\Omega_{q,a}$ (and similarly for the other regions). For the opposite-spin electrons already the first term of this expansion, the on-top pair density $\rho_2^{\alpha\beta}(\vec{r}_a,\vec{r}_a)$, that is, at the electron–electron coalescence, is non-vanishing. Thus, the $q_{\alpha\beta}$-restricted pair population can be approximated by:

$$\zeta_{q,CI}^{\alpha\beta}(\vec{r}_a) \approx\; V(\Omega_{q,a})^2\;\rho_2^{\alpha\beta}(\vec{r}_a,\vec{r}_a)\;+X(\Omega_{q,a}) \tag{7}$$

The first term of Eq. 7 is proportional to the squared volume $V(\Omega_{q,a})$ of the region $\Omega_{q,a}$. The second term, $X(\Omega_{q,a})$, collects all the other integrals from the Taylor expansion of the pair density that are proportional to the powers of $V(\Omega_{q,a})$ higher than 2.

As already mentioned, the regions $\Omega_{q,a}$ are controlled by the condition that the product of the α-spin and β-spin charges, $q_\alpha q_\beta$, yields for all regions the same value. If $q_\alpha q_\beta$ is chosen small enough then the squared volume of any region $\Omega_{q,a}$ is inversely proportional to the product of the α-spin and β-spin electron densities:

$$V(\Omega_{q,a})^2 \;\approx\; \frac{q_\alpha q_\beta}{\rho_\alpha(\vec{r}_a)\rho_\beta(\vec{r}_a)}. \tag{8}$$

Furthermore, for sufficiently small $q_\alpha q_\beta$ all integrals in $X(\Omega_{q,a})$ can be omitted, because they are proportional to higher powers of $q_\alpha q_\beta$ (thus, becoming negligibly small).

The expansion of the on-top pair density in the molecular orbital basis and the neglect of the higher order term $X(\Omega_{q,a})$, cf. Eqs. 6 and 7, lead to the approximate expression for the $q_{\alpha\beta}$-restricted pair population $\zeta_{q,CI}^{\alpha\beta}(\vec{r}_a)$ for CI wavefunction:

$$\zeta_{q,CI}^{\alpha\beta}(\vec{r}_a) \approx \frac{1}{2}\;q_\alpha q_\beta\;\frac{1}{\rho_\alpha(\vec{r}_a)\rho_\beta(\vec{r}_a)} \times \sum_{i,k}^{\alpha}\sum_{j,l}^{\beta} P_{ij,kl}\;\phi_i(\vec{r}_a)\phi_j(\vec{r}_a)\phi_k(\vec{r}_a)\phi_l(\vec{r}_a) \tag{9}$$

The actual value of $\zeta_{q,CI}^{\alpha\beta}(\vec{r}_a)$ depends on the choice of the fixed charge product $q_\alpha q_\beta$. We define ELIA, $\Upsilon^{\alpha\beta}(\vec{r}_a)$, in the following way:

$$\Upsilon^{\alpha\beta}(\vec{r}_a) = c_q\;\zeta_{q,CI}^{\alpha\beta}(\vec{r}_a). \tag{10}$$

The factor $c_q = 2/(q_\alpha q_\beta)$ compensates the $q_\alpha q_\beta$ dependency of $\zeta^{\alpha\beta}_{q,CI}(\vec{r}_a)$. The factor 2 originates from $\rho_2^{\alpha\beta} = \rho_2^{\beta\alpha}$ (instead, we could insert the sum $\zeta^{\alpha\beta}_{q,CI}(\vec{r}_a) + \zeta^{\beta\alpha}_{q,CI}(\vec{r}_a)$ into the definition for ELIA).

ELIA describes the opposite-spin pair population. Considering Eqs. 5, 7, and 8 it is clear that, in case of the fixed charge product condition, ELIA is approximated by the on-top value of the correlation factor, that is, $1 + f^{\alpha\beta}(\vec{r}_a, \vec{r}_a)$. Thus, the correlation factor merely serves to approximate this functional in case of the fixed charge product condition. Notice that ELI, describing the same-spin pair population, is approximated by the curvature of the same-spin correlation factor instead (because $f^{\alpha\alpha}(\vec{r}_a, \vec{r}_a) = 0$), cf. Part I.

Choosing another restriction for the volumes of the regions Ω would still yield an opposite-spin pair population, but now for space decomposition (into the regions Ω) possibly very different form the one used in the present work. Such pair populations would not be approximated by the correlation factor any more. For instance, examining the opposite-spin pair population using regions of fixed total charge, that is, constant $q_\alpha + q_\beta$, would be approximated by the opposite-spin correlation factor only in the closed shell system (where $q_\alpha = q_\beta$). Otherwise, for open shell systems:

$$V(\Omega_{q,a}) \approx \frac{q_\alpha + q_\beta}{\rho_\alpha(\vec{r}_a) + \rho_\beta(\vec{r}_a)}. \tag{11}$$

This yields:

$$\zeta_q^{\alpha\beta}(\vec{r}_a) \approx \frac{1}{2}(q_\alpha + q_\beta)^2 \frac{\rho_\alpha(\vec{r}_a)\rho_\beta(\vec{r}_a)}{[\rho_\alpha(\vec{r}_a) + \rho_\beta(\vec{r}_a)]^2} \times \left[1 + f^{\alpha\beta}(\vec{r}_a, \vec{r}_a)\right]. \tag{12}$$

In this case the opposite-spin pair population is approximated by the correlation factor modulated by α-spin and β-spin density dependent ratio.

3 Results

We present for the first time the characteristic behavior of the electron localizability indicator for antiparallel-spin pairs. Because ELIA is dependent on the on-top pair density, cf. Eq. 7, the quality of the on-top pair density is crucial for the evaluation of ELIA. The CI ansatz exhibits relatively slow convergence for the Coulomb-hole shape [10]. This is especially true for the value of the on-top pair density [11]. We therefore compare ELIA results for the ^1S state of He atom using CI wavefunctions of increasing quality on the one hand with those from parametrized Hylleraas wavefunctions [12] on the other. The latter show the correct behavior at electron–electron coalescence and is used as a bench-mark in the series of calculations. A few additional examples merely serve to elucidate the principles of our approach.

The quantum chemical calculations were performed with the Gaussian 98 package [13]. ELIA was computed from the Gaussian results with the program DGrid [14] which was extended to evaluate the CI vectors and configuration lists according to the formula 9. The localizability basins were determined with the program Basin [15].

3.1 He atom

In the ground state ^1S of the He atom we have two electrons with antiparallel spin (i.e., in this case it is not possible to calculate ELI, where two same-spin electrons are needed). Three complete active space self-consistent field (CASSCF) calculations were performed using the correlation-consistent basis set cc-pVQZ with different number of orbitals in the active space. CASSCF(2,5) includes the atomic orbitals 1s, 2s, and 2p, whereas for CASSCF(2,14) and CASSCF(2,30) the number of atomic orbitals was successively increased to 1s, 2s, 2p, 3s, 3p, 3d, 4s, 4p, 4d, and 4f. ELIA was computed from the resulting correlated wavefunctions.

In addition, ELIA was determined from the on-top pair density and the electron density given by the 20-parameter Hylleraas function of Hart and Herzberg [16]. Hylleraas functions explicitly include the distance between the electrons [12]. The resulting CASSCF energies are about 6.4 mHartree (CASSCF(2,5)), 2.3 mHartree (CASSCF(2,14)), and 1.3 mHartree (CASSCF(2,30)), respectively, above the energy of −2903.72 mHartree for the Hylleraas function.

Figure 2 displays ELIA for the discussed wavefunctions. All curves show a maximum at the distance of about 13–23 pm from the nucleus. The diagrams for the CASSCF wavefunctions exhibit more or less pronounced oscillations following the respective ELIA maximum. It is obvious that the more orbitals used in the CASSCF the closer the ELIA curves nestle against the Hylleraas result. This is especially evident at higher distances from the nucleus.

As described in the Theory section, for a HF wavefunction the probability to find an opposite-spin electron pair in a fixed charge region equals the charge product $q_\alpha q_\beta$ (this we have attributed to the "uncorrelated" motion of electrons). In

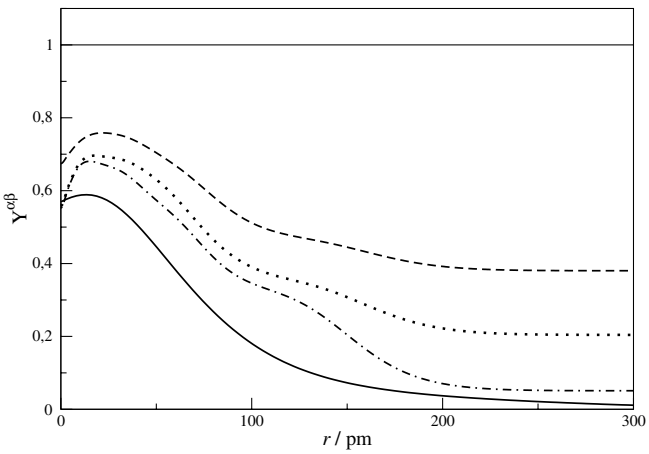

Fig. 2 ELIA for the ^1S state of helium. *Dashed line*: CASSCF(2,5); *dotted line*: CASSCF(2,14); *dash-dotted line*: CASSCF(2,30); *solid line*: 20-parameter Hylleraas function. The *straight line* for $\Upsilon^{\alpha\beta} = 1$ depict the HF case

this case ELIA would be equal to 1 at any distance from the nucleus, cf. the straight line in Fig. 2. The above results for the He atom show, that in the correlated case the opposite-spin electrons are allowed to avoid each other more than in the HF case. Higher ELIA values are found only in regions where the avoidance of the opposite-spin pairing is less pronounced.

3.2 Ne atom

The CASSCF calculations for the ground state ^1S of the Ne atom were performed with the cc-pVTZ basis set. For the CASSCF(8,8) the atomic orbitals 2s, 2p, 3s, and 3p were used in the active space. For the CASSCF(10,9) also the 1s orbital was included into the active space.

The ELIA diagrams for the two resulting correlated wavefunctions are shown in Fig. 3. The CASSCF(8,8) and CASSCF (10,9) curves exhibit a local minimum at the distances of 21.1 and 20.9 pm, respectively, from the nucleus. The integration of the electron density within the sphere of this radius yields the respective charges of 2.71 and 2.69 electrons. In both cases this region can be attributed to the first atomic shell. It is followed by an ELIA maximum marking the second atomic shell. The next (shallow) ELIA minimum is located around 151 pm from the nucleus (a sphere of this radius encompases the charge of 9.96 electrons, that is, over 99% of the total electronic charge).

In the CASSCF(8,8) the 1s orbital is not included in the active space. The dashed curve in the inset diagram in Fig. 3 shows that for this calculation the suppression of the pairing of the opposite-spin electrons is somewhat less pronounced in comparison to the CASSCF(10,9) calculation. We can speculate that the proper treatment of the inner shell electrons could lead to significant suppression of the pairing accompanied by a shift of the ELIA minimum, thus changing the electron count in the first shell (ELI yields the radius of 15.7 pm and the count of 2.16 electrons for the first atomic shell using the CASSCF(10,9) wavefunction).

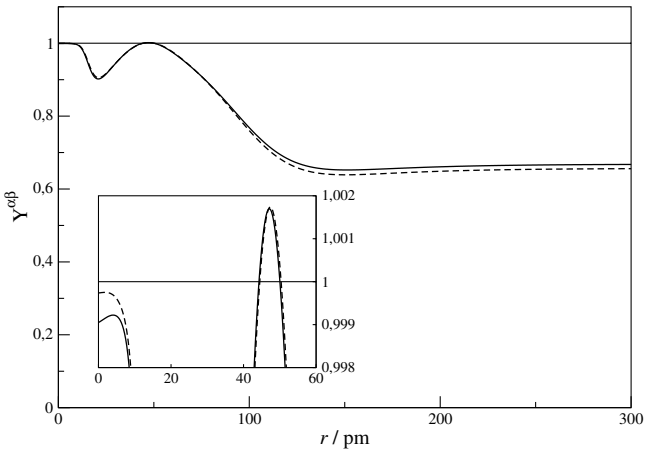

Fig. 3 ELIA for the ^1S state of neon. *Dashed line*: CASSCF(8,8); *solid line*: CASSCF(10,9). The *straight line* for $\Upsilon^{\alpha\beta} = 1$ depict the HF case

The ELIA maximum marking the second atomic shell is slightly above 1, that is, above the value for the uncorrelated HF-like motion of the opposite-spin electrons, cf. the inset in Fig. 3. Consequently, the value of the correlation factor $f^{\alpha\beta}(\vec{r}_a, \vec{r}_a)$ at the electron–electron coalescence has changed its sign at the examined position. Future calculations will show, whether for highly correlated wavefunctions this feature will persist or, possibly, a similar extent of pairing avoidance within the atomic shells will be observed as in the case of the He atom.

3.3 H_2 molecule

The ground state $^1\Sigma_g^+$ of the H_2 molecule is occupied by two electrons with opposite spins. In case of ELI, see Part I, the absence of the same-spin electron pair, yielding zero q_σ-restricted pair population, conceals the bond descriptor for both, the correlated and uncorrelated wavefunctions. In contrast to ELI, the bond descriptor emerges for ELIA determined from a correlated wavefunction.

Figure 4a shows ELIA for the H_2 molecule (bond distance of 75 pm) computed from the CASSCF(2,6) wavefunction, that is, with 6 molecular orbitals in the active space, using the aug-cc-pVTZ basis set. The ELIA maximum between the hydrogen atoms represents the bond descriptor. This feature cannot be represented by ELI, because of the lack of same-spin electron pair in the ground state of H_2 molecule. Additionally, there are high ELIA values enclosing the molecule. As in the case of atoms, those "oscillations" are due to the insufficient treatment of correlation. The basis set as well as the size of the active space in CASSCF(2,6) is not flexible enough to yield an adequate avoidance of the opposite-spin electron pairing in this region (located relatively far outside the nuclei and, therefore, likely not relevant for the bond analysis).

Performing the CASSCF(2,6) calculation with the aug-cc-pVQZ basis set (that includes f-functions) yields ELIA with high values concentrated toward the bond axis, see Fig. 4b. Nevertheless, there are still spurious ELIA maxima located along the bond axis outside the bond region.

Using the aug-cc-pVQZ basis set and the active space of 19 orbitals the CASSCF(2,19) calculation was performed and ELIA was computed from the resulting wavefunction. Figure 4c reflects the enormous reduction of ELIA values, especially in the outer regions, where ELIA continuously decreases to 0 (with slight oscillations in the very outer area). Even at the bond midpoint ELIA drops to 0.7, that is, the improved treatment of the correlation results in widespread suppression of the opposite-spin electron pairing compared to the less correlated cases. The main feature of Fig. 4c is the steady decrease of ELIA from the single maximum located at the bond midpoint (except for the oscillations at very low electron densities). The ELIA maximum at the bond midpoint represents the bond descriptor.

At the restricted HF level the Lewis model of chemical bonding is related to pairwise occupation of orbitals by elec-

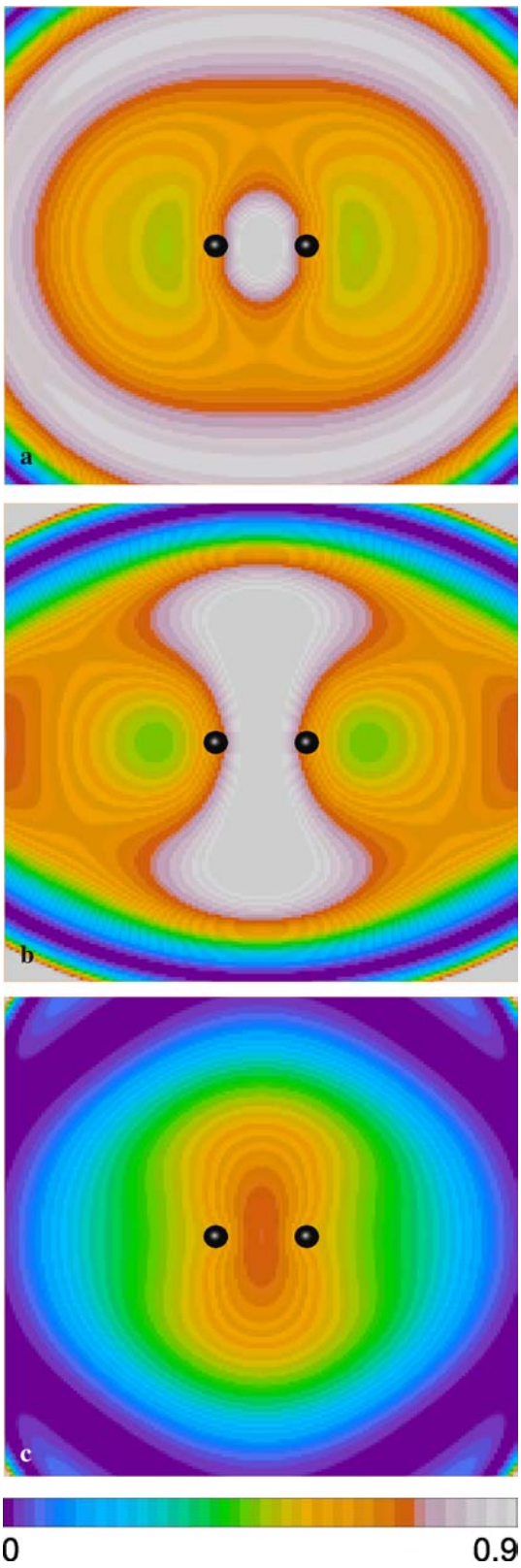

Fig. 4 ELIA for the ^1S state of the H_2 molecule. **a** CASSCF(2,6) using the aug-cc-pVTZ basis set; **b** CASSCF(2,6) using the aug-cc-pVQZ basis set; **c** CASSCF(2,19) using the aug-cc-pVQZ basis set. The *black spheres* represent the nuclei. The ELIA colormap is at the bottom

trons of opposite spin. For correlated wavefunctions this correspondence is no more so evident, because a huge amount of configurations needs to be taken into account. In this case ELIA can be regarded as a direct manifestation of the Lewis model of chemical bonding in real space, showing regions of space where the pairing of opposite-spin electrons is emphasized (unlike ELI, for which the manifestation is just indirect, as it shows region of space where the pairing of same-spin electrons is less pronounced).

3.4 N_2 molecule

The $^1\Sigma_g^+$ state of the N_2 molecule was computed at the bond distance of 111 pm [17] using the aug-cc-pVTZ basis set. As in Part I, the CASSCF(10,8) calculation was performed with the active space consisting of the orbitals $2\sigma_g$, $3\sigma_g$, $2\sigma_u$, $3\sigma_u$, $1\pi_{ux}$, $1\pi_{uy}$, $1\pi_{gx}$, and $1\pi_{gy}$. For the CASSCF(10,9) the active space was extended with the $4\sigma_g$ orbital. The CASSCF(10,9) calculation involved 15876 Slater determinants.

Figure 5a shows ELIA for the CASSCF(10,8) calculation. The bonding features expected for the N_2 molecule are clearly recognizable. The 0.999-localization domains along the bond axis visualize the atomic cores separated by the bond region. Two localization domains in the opposite directions are located in the lone-pair regions. The corresponding ELIA maxima (attractors) are relatively far outside, that is, the localization domains are not solely contained in the computed area. At higher ELIA values the localization domain marking the bond region (also not solely contained in the computed area) opens at the bond midpoint, surrounding the bond axis (i.e., there is a ring-attractor, thus, no ELIA maximum at the bond midpoint).

The extension of the active space by the $4\sigma_g$ orbital suppresses the ELIA values in the outer regions, cf. Fig. 5b for the CASSCF(10,9) calculation. The ELIA maxima, which serve as the lone-pair descriptors, are positioned closer to the nuclei. The corresponding 0.999-localization domains are solely contained in the computed area. Similarly for the 0.999-localization domain in the bond region, forming a thin disc around the bond axis. As for the CASSCF(10,8) calculation, there is no ELIA maximum at the bond midpoint, that is, ELIA shows a ring-attractor for the nitrogen bond.

The electron counts for the ELIA basins differ significantly from the ones for the ELI basins, cf. Part I. For the CASSCF(10,9) calculation the ELIA bond basin encompases the charge of 4.42 electrons, which is 1 electron more than for the ELI bond basin. For the lone-pair basin ELIA yields the count of 2.21 electrons, in contrary to the 3.15 electrons for the ELI. The core basin shows somewhat higher count of 2.58 electrons, similarly to the Ne atom described above.

3.5 F_2 molecule

For the ground state $^1\Sigma_g^+$ of the F_2 molecule two calculations were performed at the bond distance of 146 pm [17]. The CASSCF(14, 9) calculation with the aug-cc-pVTZ basis

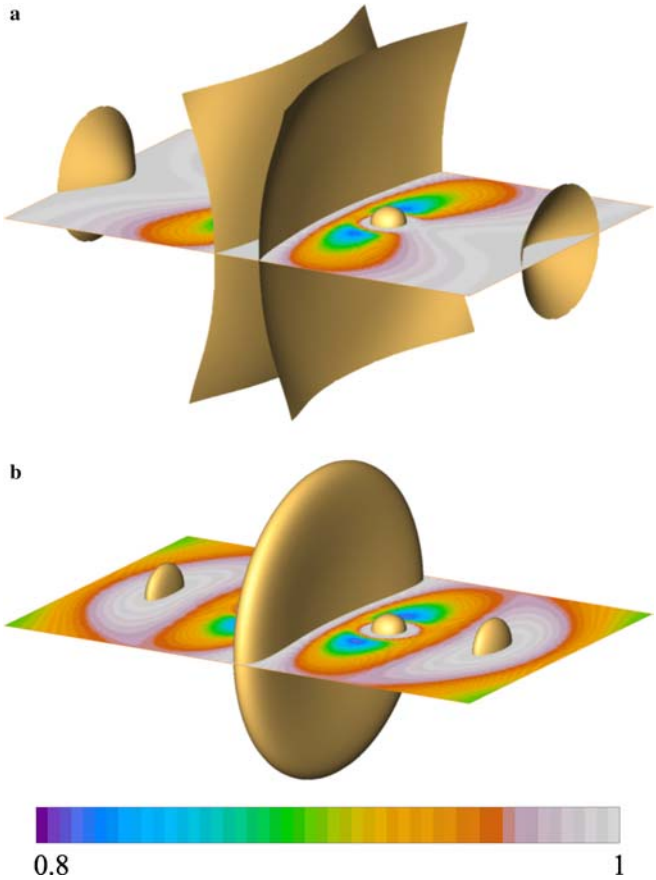

Fig. 5 ELIA for the ground state $^1\Sigma_g^+$ state of the N_2 molecule (0.999-localization domains). **a** CASSCF(10,8) ; **b** CASSCF(10,9). The colormap applies to the slices

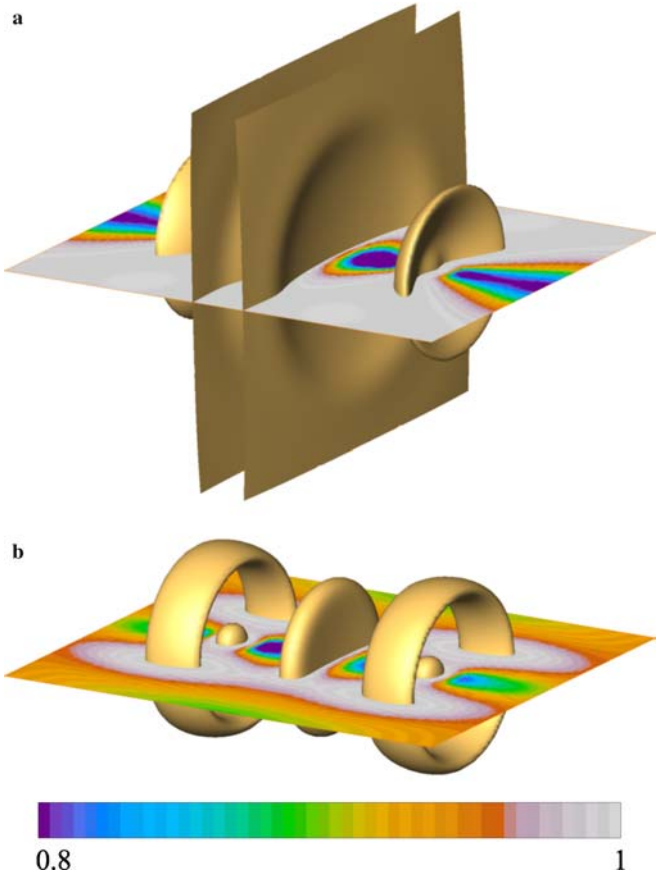

Fig. 6 ELIA for the ground state $^1\Sigma_g^+$ state of the F_2 molecule. **a** 0.9999-localization domains for the CASSCF(14,9) using the aug-cc-pVTZ basis set; **b** 0.999-localization domains for the CASSCF(14,11) using the cc-pVDZ basis set. The colormap applies to the slices

set and the active space consisting of the orbitals $2\sigma_g$, $3\sigma_g$, $2\sigma_u$, $3\sigma_u$, $4\sigma_u$, $1\pi_{ux}$, $1\pi_{uy}$, $1\pi_{gx}$, and $1\pi_{gy}$ involved 1296 Slater determinants. For the CASSCF(14,11) calculation the cc-pVDZ basis set and the active space consisting of the orbitals $2\sigma_g$, $3\sigma_g$, $2\sigma_u$, $3\sigma_u$, $4\sigma_u$, $1\pi_{ux}$, $1\pi_{uy}$, $2\pi_{ux}$, $2\pi_{uy}$, $1\pi_{gx}$, and $1\pi_{gy}$ was used. This calculation involved 108900 Slater determinants.

Figure 6a shows ELIA for the CASSCF(14,9) calculation. The open 0.9999-localization domain visualizes the bond region. It is situated around the ELIA maximum at the bond midpoint. The two closed 0.9999-localization domains are located in the core and lone-pair region. The core region can almost be anticipated from the shape of these localization domains. Nevertheless, separate localization domains for each core do not emerge at higher ELIA values (i.e., there is no separate ELIA maximum for the core region). Remarkable is also the pronounced suppression of the opposite-spin pairing along the bond axis (except the core as well as the bond midpoint regions).

In the CASSCF(14,11) calculation the active space was extended by the bonding $2\pi_u$ orbitals. Compared to the CASSCF(14,9) calculation the pairing of the opposite-spin electrons is suppressed outside the bond axis, cf. Fig. 6b. The 0.999-localization domains display separate core regions. For the core basin the count of 2.78 electrons was found. The ring-shaped ELIA domains around each core visualize the lone-pair regions. The lone-pair basin contains the charge of 5.79 electrons. The disc-shaped localization domain between the cores visualizes the bond region. It is located around the ELIA maximum at the bond midpoint. The ELIA bond basin contains the charge of 0.86 electrons.

4 Conclusions

The electron localizability indicator for ELIA is a functional of the opposite-spin electron pair density. ELIA is uniquely defined for any approach that yields the opposite-spin electron pair density. It describes the local correlation of motion of opposite-spin electrons. ELIA yields information only if the Coulomb correlation between the opposite-spin electrons is included in the quantum chemical calculation. For HF wavefunction the ELIA yields a constant value for all the regions. This reflects the fact that at this level of theory the motion of electrons with opposite spins is “uncorrelated”. This behavior differs significantly from the one of ELI, which shows distinctly structurized topology already at the

HF level. The ELIA topology becomes far more interesting for correlated wavefunctions. Then, the motion of opposite-spin electrons is correlated, yielding distinctive regions of space where the electrons tend to form antiparallel-spin pairs. Such regions can be connected with atomic shells and descriptors of the bonding situation.

Similarly to ELI, ELIA reveals the atomic shell structure as illustrated on the example of the Ne atom. It was shown on the examples of H_2, N_2, and F_2 molecules that ELIA bears information about the chemical bonding. Moreover, ELIA can be regarded as a quantum mechanical manifestation of the Lewis model of chemical bonding in real space. For the singlet state of the He atom the comparison of ELIA computed from Hylleraas functions with ELIA for CASSCF calculations at different level of correlation reveals information about the quality of the analyzed wavefunctions.

Acknowledgements This study was supported by Deutsche Forschungsgemeinschaft (SPP 1166). K.P. acknowledges the Young Scientist Fellowship from the Foundation for Polish Science and extends her thanks to Max-Planck Society for research fellowship.

References

1. Kohout M, Pernal K, Wagner FR, Grin Y (2004) Theor Chem Acc 112:453
2. Becke AD, Edgecombe KE (1990) J Chem Phys 92:5397
3. Savin A, Jepsen O, Flad J, Andersen OK, Preuss H, von Schnering HG (1992) Angew Chem 104:186
4. Lewis GN (1916) J Am Chem Soc 38:762
5. Kohout M (2004) Int J Quantum Chem 97:651
6. Löwdin, P-O (1955) Phys Rev 97:1474
7. Parr RG, Yang W (1989) Density-functional theory of atoms and molecules. Oxford University Press, Oxford
8. McWeeny R, Mizuno Y (1961) Proc Roy Soc Lond 259:554
9. Kutzelnigg W (2002) Einführung in die Theoretische Chemie. Wiley-VCH Verlag GmbH, Weinheim
10. Kutzelnigg W, Morgan III JD (1992) J Chem Phys 96:4484
11. Bak KL, Halkier A, Jorgensen P, Olsen J, Helgaker T, Klopper W (2001) J Mol Struct 567–568:375
12. Hylleraas EA (1929) Z Physik 54:347
13. Frisch MJ, Trucks GW, Schlegel HB, Scuseria GE, Robb MA, Cheeseman JR, Zakrzewski VG, Montgomery JA Jr, Stratmann RE, Burant JC, Dapprich S, Millam JM, Daniels AD, Kudin KN, Strain MC, Farkas O, Tomasi J, Barone V, Cossi M, Cammi R, Mennucci B, Pomelli C, Adamo C, Clifford S, Ochterski J, Petersson GA, Ayala PY, Cui Q, Morokuma K, Malick DK, Rabuck AD, Raghavachari K, Foresman JB, Cioslowski J, Ortiz JV, Baboul AG, Stefanov BB, Liu G, Liashenko A, Piskorz P, Komaromi I, Gomperts R, Martin RL, Fox DJ, Keith T, Al-Laham MA, Peng CY, Nanayakkara A, Gonzalez C, Challacombe M, Gill PMW, Johnson B, Chen W, Wong MW, Andres JL, Gonzalez C, Head-Gordon M, Replogle ES, Pople JA (1998) Gaussian 98, Revision A.7, Gaussian Inc., Pittsburgh
14. Kohout M (2004) program DGrid, Version 2.4. Max-Planck-Institut für Chemische Physik fester Stoffe, Dresden
15. Kohout M (2004) program Basin, Version 2.4. Max-Planck-Institut für Chemische Physik fester Stoffe, Dresden
16. Hart JF, Herzberg G (1957) Phys Rev 106:79
17. Peterson KA, Kendall RA, Dunning TH Jr (1993) J Chem Phys 99:9790